The 40m radiotelescope at the 87-110 GHz band after holography

P. de Vicente

Informe Técnico IT-OAN 2012-09

Revision history

Version	Date	Author	Updates
1.0	03-02-2012	P. de Vicente	First version

Contents

1 Introduction

The first set of holographic measurements and panel adjustements of the 40 m radiotelescope primary reflector finished in January 2012. According to López (2012) the primary reflector surface has an error budget of ~ 190 μm. This report summarizes the most important parameters of the telescope obtained from continuum observations after the adjustment. The last section includes estimations from observations prior to the holographic measurements and the surface adjustement to display its evolution.

2 Measurements

The telescope uses a single polarization 3 mm receiver borrowed from IRAM that was previously used at the Plateau de Bure interferometer. See Cordobés et al. (2009) and de Vicente et al (2010a) for a description. All pending tasks with the 3 mm receiver mentioned in report IT-OAN 2010-16 were solved. The most important, the lack of reliability of the remote hot-load control system, was fully fixed. The IF attenuators were also correctly set so that in all circumstances (hot and cold loads and sky) the power detectors (PBE and FFT) worked in a linear regime. More observations were performed at 87 GHz after replacing the vertex membrane (de Vicente et al. 2011) and can be considered the reference ones before holography adjustments.

Observations in the continuum towards Mars, Venus, Saturn and 3C84 were performed at 85, 87, 90, 100 and 110 GHz between January 19th and March 26th 2012. Observations were done with different configurations (millimeter polarizer installed and removed, and different focus setups). Not all sources were observed at all frequencies. Observations consisted on double on the fly pointing scans 150 arcsecs wide interleaved with calibration hot-cold load scans and a focus scan along the Z axis every 6 other scans approximately. The focus was corrected manually and the pointing was automatically corrected from a macro script. Skydips were performed from time to time. Continuum maps towards the sources were also performed.

3 Skydips

Skydips allow to determine the forward efficiency and the opacity of the atmosphere at the frequency of observation. A skydip is a scan in which the antenna sweeps from the horizon to the zenith while taking data in the continuum. Fig. 1 shows a collection of skydips performed at 4 different frequencies: 86, 90, 100 and 110 GHz, in the first epoch of observations (with the millimeter polarizer installed).

The antenna temperature of the sky (T^a_{sky}) in a skydip can be written as:

$$T^a_{sky} = \eta_f T_{atm}(1 - e^{-\tau_0 A}) + T_{rx} + T_g(1 - \eta_f) \quad (1)$$

where η_f is the forward eficciency and represents the fraction of radiation that enters the horn from the front part of the antenna. T_{atm} is the atmospheric temperature and, as an approximation, can be considered to be the ground temperature minus 40 degrees. τ_0 is the atmospheric opacity in the zenith and A the number of airmasses (1 towards the zenith). T_{rx} is the receiver

temperature and T_g the ground temperature. The dependency of the previous expression on elevation allows to determine the forward efficiency and the opacity towards the zenith.

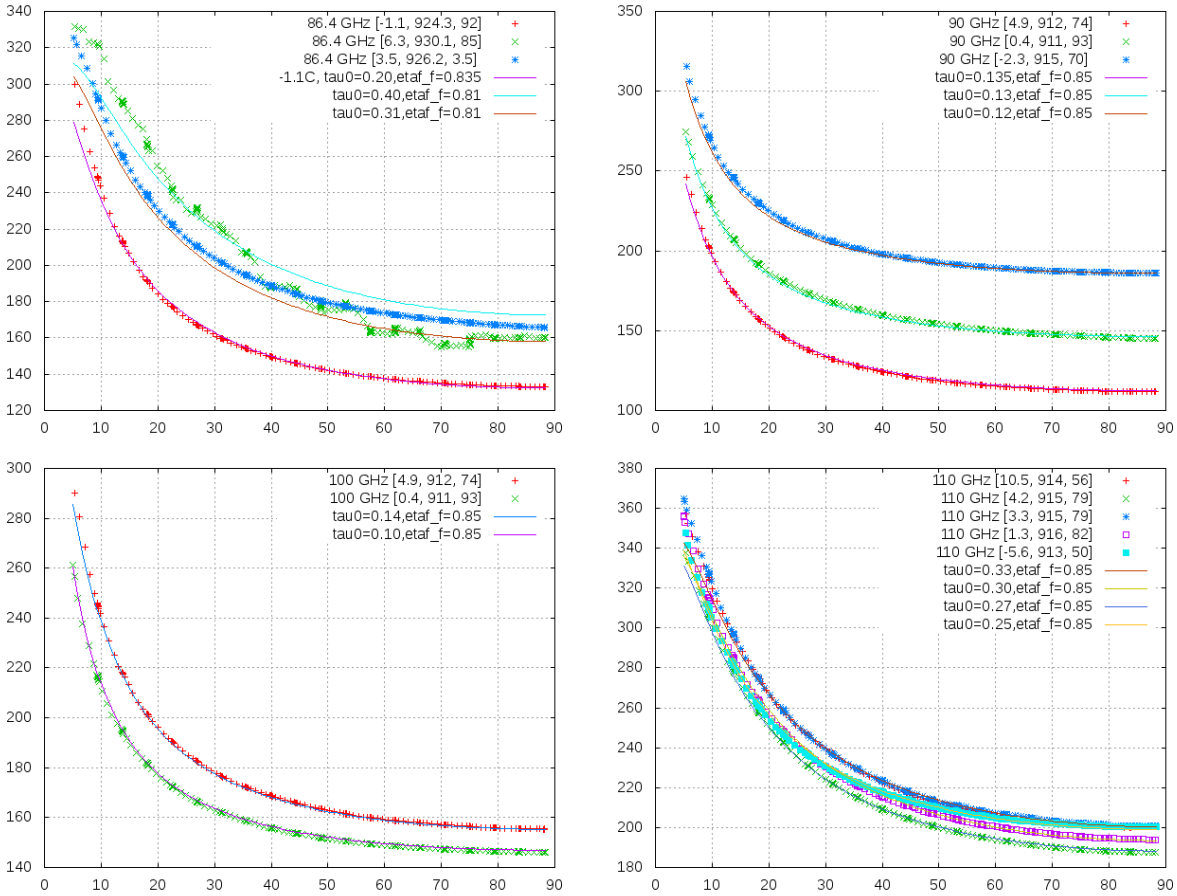

Figure 1: *Skydips for the 3 mm band at 86, 90, 100 and 110 GHz. The polarizer was installed*

All fits have been done manually. Free parameters were the opacity towards the zenith and the forward efficiency. The main boundary condition for the forward efficiency is that it should be the same at all 3 millimeter frequencies. The starting value for the opacity was obtained from ATM, a theoretical model which computes it from the ammount of precipitable water in the atmosphere. Precipitable water was obtained from weather parameters in the environment of the 40 m radiotelescope (see de Vicente et al. 2010a, section 5). The forward efficiency obtained was 0.85. The opacity varied in all cases and showed some discrepancy with the theoretical models which is larger at higher frequencies. Table 1 contains a summary of the opacities for all skydips computed from AM, ATM and fitted from the skydips.

3.1 Efficiency of the vertex membrane revised

The 40 m radiotelescope has a membrane in the vertex whose effect should be included into the previous expression. Let the efficiency of the membrane be η_m. The previous expression should be modified taking into account that radiation coming from forward is partially absorbed

Sky Freq	H_2O	τ_z		
	[mm]	AM	ATM	Skydip
86	10.3	0.12	0.12	0.20
86	15.7	0.18	0.18	0.40
86	14.3	0.16	0.17	0.31
90	12.5	0.14	0.15	0.13
90	11.6	0.14	0.14	0.13
90	7.2	0.11	0.09	0.12
100	11.6	0.10	0.17	0.14
100	6.3	0.10	0.10	0.10
110	12.7	0.17	0.25	0.31
110	12.0	0.18	0.24	0.30
110	11.0	0.17	0.22	0.30
110	10.8	0.17	0.22	0.27
110	4.1	0.13	0.11	0.25

Table 1: *Ammount of precipitable water in mm and estimated zenital opacities (using two models: AM and ATM) and from a skydip fit. Millimeter polarizer was installed*

by the membrane, but the membrane also generates radiation as a black body at the ambient temperature (T_g). Hence the membrane acts as a slab of material in the way of the radiation:

$$\begin{aligned} T^a_{sky} &= \eta_f T_{atm}(1-e^{-\tau_0 A})\eta_m + T_{rx} + T_g(1-\eta_f)\eta_m + T_g(1-\eta_m) \\ &= \eta_f\,\eta_m T_{atm}(1-e^{-\tau_0 A}) + T_{rx} + T_g(1-\eta_f\,\eta_m) \\ &= \eta'_f T_{atm}(1-e^{-\tau_0 A}) + T_{rx} + T_g(1-\eta'_f) \end{aligned} \quad (2)$$

and the expression is exactly the same as expression 1, where the new forward efficiency $\eta'_f = \eta_f\eta_m$ is lower than the one without membrane η_f and absorbs the efficiency of the membrane.

The membrane efficiency was estimated in report OAN 2011-4 to be 0.82 from observations towards Venus with and without the membrane. That report also provided an efficiency of 0.95 from an observation towards Venus inserting a slab of the same material as the membrane in front of the ray path.

According to 2 a membrane efficiency of 0.82 is not possible. If the forward efficiency we determine is 0.85, then,

$$\begin{aligned} \eta'_f &= \eta_m\,\eta_f \\ 0.85 &= 0.82\,\eta_f \end{aligned}$$

which implies that the 40 m forward efficiency without membrane is 1.03. Since this value is wrong we have recomputed the efficiency from skydips done with and without the new membrane in 2011. Skydips with one setup and the other were performed then with a time lapse of 6.5 hours with similar weather conditions.

The forward efficiency determined in IT OAN-2011-4 without membrane was: 0.72 ± 0.01

and with the new membrane: 0.67 $\pm$ 0.01. Therefore:

$$\eta_m \quad = \eta'_f/\eta_f = 0.67/0.72 = 0.93$$

This estimation, 0.93, is closer to 0.95, determined from the last method (inserting a slab of material in the ray path) described above. Hereafter we will consider the efficiency of the membrane of the vertex to be 0.94 $\pm$0.01

4 Polarizer efficiency

In front of the receiver there is a $\lambda/4$ polarizer (see Fig. 2). It is a circular grooved teflon plate that selects circular polarization and converts it to linear polarization. The sense of rotation of the polarization (right or left) is achieved by rotating the plate 90 degrees. Currently the polarization is left circular. We have done some measurements with the plate on and off to estimate its attenuation.

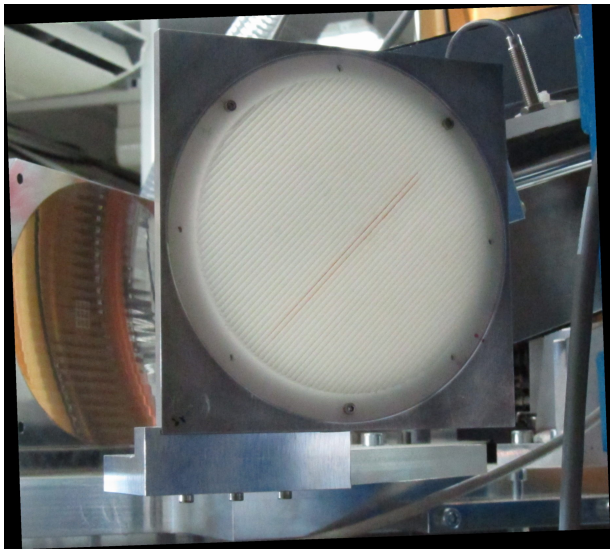

Figure 2: $\lambda/4$ *polarizer in front of the mm receiver.*

Fig. 3 shows the antenna temperature towards Mars and Venus at 90.8 GHz with the polarizer inserted and removed. Apparently there is no significant difference between both configurations. In order to estimate an upper limit of the difference betwen both of them we have averaged values for elevation ranges between 30 and 60 degrees for Venus and 20 to 60 degrees for Mars. The average antenna temperature towards Venus with polarizer is 31.7 K with polarizer and 36.4 K without polarizer, the antenna temperature for Mars with polarizer is 12.6 and without polarizer 12.9. The efficiency according to the previous differences would be 0.87 and 0.97. The antenna temperature difference for Venus is consequence of the big antenna temperature drop seen with the polarizer close to the culmination of the sourcei (see Fig. 3).

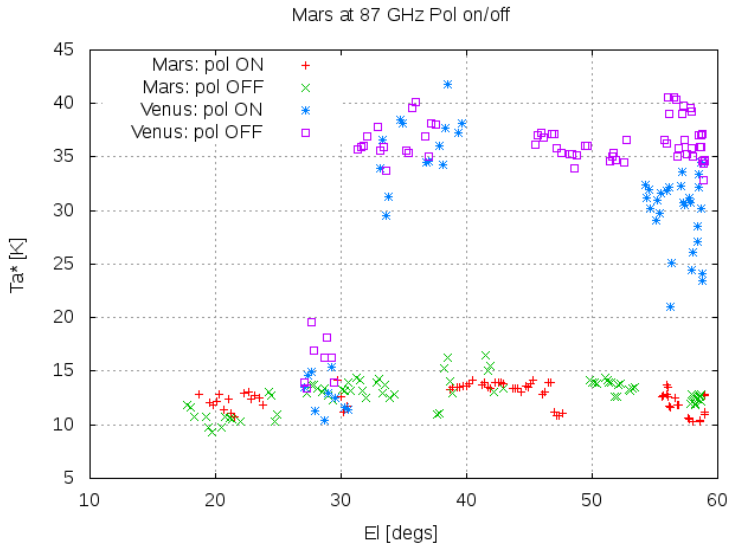

Figure 3: *Antenna temperature towards Mars and Venus with the polarizer inserted and removed as a function of elevation.*

An alternative way to estimate the efficiency of the polarizer is to do a skydip with and without the polarizer in front of the ray path and compute it from the system temperature difference between both configurations. Fig. 4 shows two skydips fo each case. The difference between both skydips towards the zenith is 8±1 K.

According to the equation of radiative transport:

$$\begin{aligned} T_{sys}(pol) &= e^{-\tau}T_{sksp} + (1-e^{-\tau})T_{amb} + T_r & (3)\\ &= \eta_p T_{sksp} + (1-\eta_p)T_{amb} + T_r & (4)\\ T_{sys} &= T_{sksp} + T_r & (5) \end{aligned}$$

where we assume that the τ is the opacity of the polarizer which behaves as a black body at ambient temperature (T_{amb} in the receiver cabin. $T_{sys}(pol)$ and T_{sys} are the system temperature with and without polarizer. The efficiency of the polarizer, η_p is:

$$\eta_p = e^{-\tau} \quad (6)$$

and we are assuming that T_{sksp} is the contribution to the system temperature once substracted the receiver temperature and before the polarizer. Rigorously, it is not the sky temperature, since the spillover is included here, but for the computations hereafter this is not important.

If we substract the system temperature with and without polarizer, we get:

$$\Delta Tsys = (1-\eta_p)(T_{amb} - T_{sksp}) \quad (7)$$

and in our case towards the zenith, $T_r = 120$ K,

$$8 = (1-\eta_p)\,(291 - (184 - 120)) = (1-\eta_p)\,227 \quad (8)$$

hence

$$\eta_p = \sim 0.965 \tag{9}$$

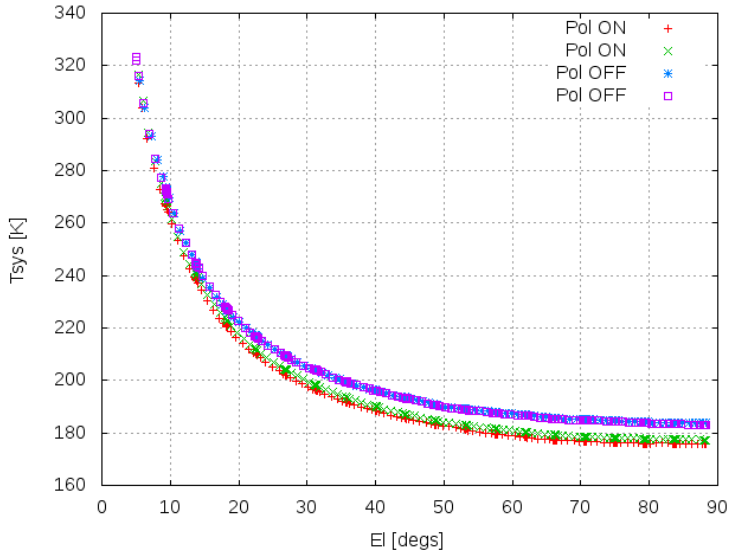

Figure 4: *Skydips at 91 GHz with and without the polarizer.*

4.1 Skydips without the polarizer

We have performed skydips without the millimeter polarizer at 86, 90 and 100 GHz (see Fig. 5). Results show that the 40 m forward efficiency is 0.89± 0.01 without the polarizer. This ammounts 5% more than with the polarizer. Expression 2 also applies and we can estimate the efficiency of the polarizer:

$$\eta_p = \eta_f'/\eta_f = 0.85/0.89 = 0.955 \tag{10}$$

This number is comparable to the system temperature result. Thefore, hereafter we will assume the mm polarizer has a constant efficiency along the band of 0.96 ± 0.005.

5 Forward efficiency, membrane and polarizer efficiencies

To sum up the results from the previous sections we include the estimations for the forward efficiency of the antena, and the efficiency of the membrane and the polarizer in table 2.

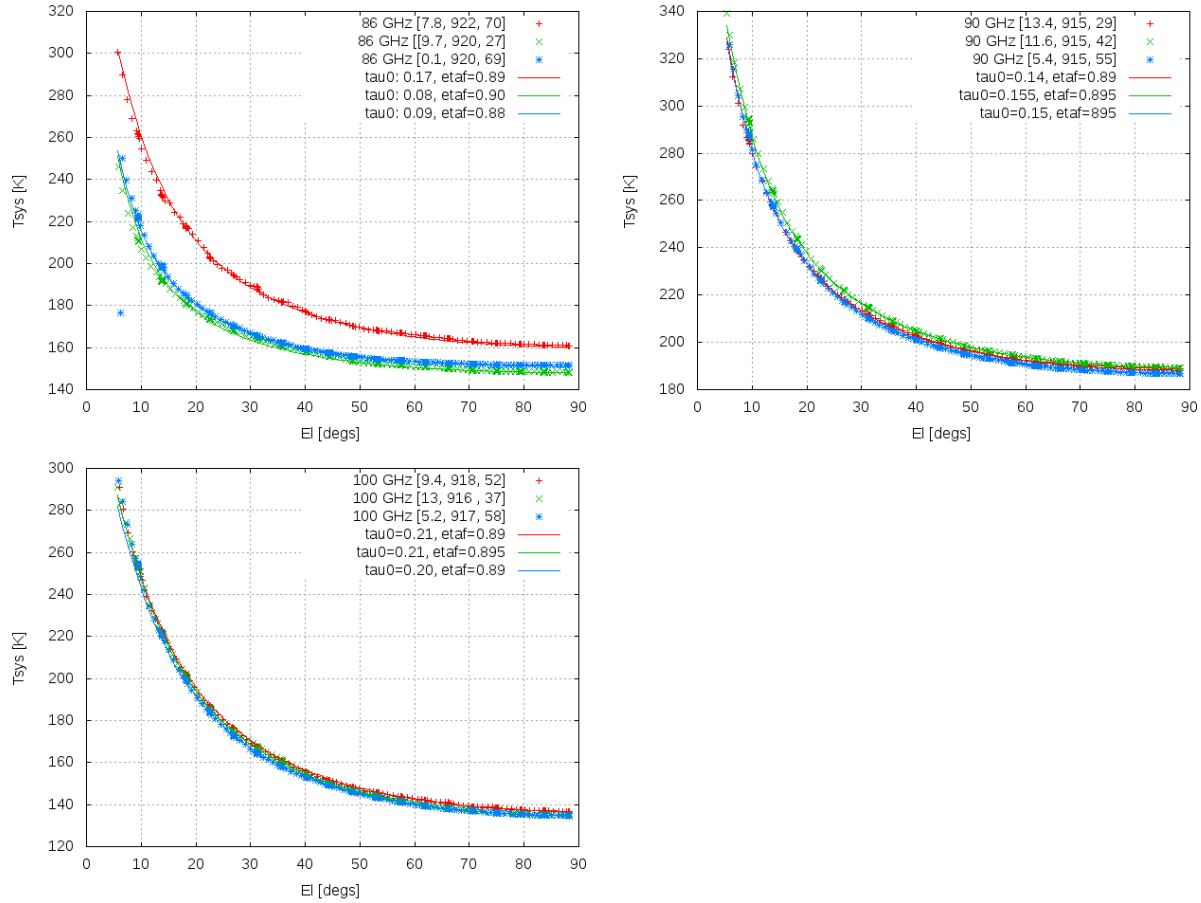

Figure 5: *Skydips for the 3 mm band at 86, 90 and 100 GHz, with the polarizer off.*

η_f	η_m	η_p	η_f^p	η_f^m
0.85	0.94	0.96	0.89	0.95

Table 2: *Forward efficiency at 3 mm, with the membrane and polarizer. Efficiency of the membrane and of the polarizer. The last two columns are estimations of the forward efficiency of the antenna without the mm polarizer, and without membrane and polarizer.*

6 Apperture efficiency and main beam

The aperture efficiency depends on the surface error of the primary reflector (η_{m1}), subreflector (η_{m2}) and other mirrors in the Nasmyth cabin (η_{nm}). It also depends on the blocking of radiation by the legs and subreflector (η_b), the illumination of the parabola (η_i), the absorption by the membrane of the vertex (η_{mb}) and resistive losses which we will neglect. Radiation reflects on 7 mirrors in the Nasmyth cabin before arriving at the 3 mm receiver and after M2 (subreflector): M3 and M4 have a surface error of 25 μm, M22 has a surface error of 40μm, M6 and M7 have a surface error of 7μm, M8 17μm and M9 has an unknown surface error. The maximum size of mirrors M6 to M9 is 20 cm and they are grooved with a grid whose maximum depth is 150 μm to help align the system.

Hence:

$$\eta_a = \eta_{m1}\eta_{m2}\eta_{nm}\eta_b\eta_{mb}\eta_i \tag{11}$$

where

$$\eta_{nm} = \eta_{m22}\eta_{m6}\eta_{m7}\eta_{m8}\eta_{m9} \tag{12}$$

The efficiency by blockage, η_b, is 0.92 (de Vicente 1998) and the efficiency due to illumination is approximately 0.7. The efficiency of the membrane is 0.94 at 87 GHz (see previous section), and according to Malo (2010) this value is approximately constant in the 80 to 120 GHz frequency interval.

The efficiency of the mirrors depends on the surface errors and hence on the frequency of observation. It is possible to estimate this dependency using Ruze's formula:

$$\eta_{mirror} = e^{-(\frac{4\pi\sigma}{\lambda})^2} \tag{13}$$

where σ is the RMS of the surface and λ the observing wavelength in the same units as σ. The lowest efficiency for mirrors M6 to M9, if we discard the influence of the grooving, happens at the highest frequency (110 GHz) and can be considered 1.0. The combined efficiency for mirrors M2, M3, M4 and M22 is 0.992 at 110 GHz and 0.994 at 87 GHz.

When observations are performed with the polarizer its efficiency should be taken into account. Table 3 is summary of all relevant efficiencies to be taken into account when observing at 3 mm.

η_i	η_b	η_{mb}	η_{nm}	η_p
0.7	0.92	0.94	0.99	0.96

Table 3: *Efficiencies of the different elements along the 3 mm path. We have assumed all of them are constant in the 87 GHz to 110 GHz. η_i: illumination, η_b: blockage, η_{mb}: membrane, η_{nm}: nasmyth mirrors, η_p: polarizer*

Hence, if we include the polarizer:

$$\eta_a = \eta_{m1}\,0.7\,0.92\,0.94\,0.99\,0.96 = 0.57\,\eta_{m1} \tag{14}$$

The aperture efficiency can be estimated observing sources with known fluxes, like planets. Planets are bright in the mm range and their flux can be predicted from their distance to the Sun assuming that the energy they receive from the Sun is remitted as black bodies. Only planets whose size is smaller than the beam can be used as calibrators. The HPBW of the 40 m radiotelescope at 3 mm is between 17 and 21.3 arcsecs approximately and this rules out Jupiter as calibrator since its size is $\simeq$ 37 arcsecs at the time of this report. We observed Mars, Venus and Saturn in two different epochs (end of january 2012 and beginning of march 2012). Uranus and Neptune were too weak to have a good signal to noise ratio. In the first epoch the polarizer was used, while in the second the polarizer was removed.

Table 4 summarizes the HPBW of the telescope at different frequencies. Since the observations spanned several weeks, the flux varied along the observation interval. The HPBW has been estimated assuming a taper of 0.2:

$$\theta = b\frac{\lambda}{D} \simeq 1.2\frac{\lambda}{D} \tag{15}$$

Sky Freq GHz	λ [mm]	HPBW ["]
86	3.5	21.3
90	3.3	20.5
100	3.0	18.5
110	2.7	16.8

Table 4: *40 m radiotelescope HPBW for 4 different frequencies in the 3 mm range*

The aperture efficiency according to Baars (2007) is:

$$\eta_a = \frac{2K_B C_s T'_a}{AS_f} \tag{16}$$

where T'_a is the antenna temperature corrected by the atmospheric attenuation, A the radiotelescope collecting area, S_f the source flux and C_s a factor which takes into account the source brightness distribution compared to the antenna HPBW and is only valid for sources whose size is equal or smaller than the beam width:

$$C_s = \begin{cases} 1 + x^2 & \text{gaussian source} \\ \frac{x^2}{1-\exp(-x^2)} & \text{disk source} \end{cases} \tag{17}$$

where,

$$x = \frac{\theta_s('')}{1.2\,\theta_b('')} \tag{18}$$

and θ_s is the source size and θ_b the HPBW of the antenna.

For the 40 m radiotelescope we can write:

$$\eta_a = 2.197 \frac{C_s\, T'_a[\mathrm{K}]}{S_f[\mathrm{Jy}]} \tag{19}$$

The beam efficiency is the fraction of the power received by the antenna which enters the main beam. The main beam is defined to extend to the first null in the radiation pattern. It can be computed for point like sources (Baars 2007) from:

$$\eta_{mb} = \frac{\Omega_m A_g}{\lambda^2}\eta_a \tag{20}$$

$$= \frac{\pi D^2}{4}\frac{1.133}{\lambda^2}\left(\frac{1.16\lambda}{D}\right)^2 = 0.89\,1.16^2\,\eta_a \tag{21}$$

$$= 1.1976\,\eta_a \tag{22}$$

where Ω_m is beam solid angle, A_g the geometrical area, λ the observing length and D the diameter of the antenna.

Results are summarized in tables 5 (first epoch with polarizer) and 6 (second epoch without polarizer).

Freq.	Source	Flux (Jy)	Size (")	C_s	T'$_a$ (K)	T'$_a$/S (K/Jy)	η_a
85	Mars	112	$12'' \times 12''$	1.14	9.2	12.1	0.21
86	Venus	320	$14'' \times 14''$	1.16	28.8	11.1	0.23
86	Mars	100	$11'' \times 11''$	1.10	9.6	10.4	0.23
86	Saturn	173	$17.5'' \times 15.5''$	1.22	11.2	15.3	0.17
90	Venus	365	$15'' \times 15''$	1.20	16.6	22.0	0.12
90	Mars	120	$11.5'' \times 11.5''$	1.11	6.2	19.0	0.13
90	Saturn	180	$17.5'' \times 15.5''$	1.25	10.0	18.0	0.15
100	Venus	430	$15'' \times 15''$	1.25	23.5	18.2	0.15
100	Mars	150	$11.5'' \times 11.5''$	1.14	7.1	21.1	0.12
100	Saturn	225	$17.5'' \times 15.5''$	1.30	9.3	24.0	0.12
110	Venus	473	$15'' \times 15''$	1.30	23.2	20.4	0.13
110	Mars	158	$11'' \times 11''$	1.15	8.1	19.5	0.13
110	Venus	535	$15.2'' \times 15.2''$	1.31	21.8	24.5	0.12

Table 5: *Size, flux, antenna temperature (corrected by opacity), source correction, antenna temperature flux ratio and aperture efficiency for Venus and Saturn at 86.2 GHz. All data were taken at 30 degrees elevation approximately. Observations at 110 GHz were of very poor quality and should be taken with care.*

The maximum aperture efficiency at 3 mm from both observation epochs is achieved at 86 GHz: 21% $\pm$2%. The aperture efficiency at 90 GHz is 14.5% $\pm$2%, and 12.5% $\pm$2% at 100 GHz. These values have been obtained averaging values from both epochs, even thought epoch

Sky freq.	Source	Flux (Jy)	Size (")	C_s	T'$_a$ (K)	S/T'$_a$ (Jy/K)	η_a
85	Venus	320	$18.3'' \times 18.3''$	1.29	37.5	13.8	0.21
85	Mars	100	$13.8'' \times 13.8''$	1.15	10.8	14.0	0.18
85	Saturn	173	$18.3'' \times 16.8''$	1.25	13.8	13.1	0.21
90	Venus	365	$18.3'' \times 18.3''$	1.30	30.5	18.3	0.15
90	Mars	120	$13.8'' \times 13.8''$	1.16	11.0	15.7	0.16
90	Saturn	180	$18.3'' \times 16.8''$	1.27	10.2	20.1	0.15
100	Venus	677	$18.3'' \times 18.3''$	1.38	27.4	24.7	0.12
100	Mars	210	$13.8'' \times 13.8''$	1.21	10.5	20.0	0.13
100	Saturn	250	$18.3'' \times 16.8''$	1.34	9.8	25.5	0.11

Table 6: *Size, flux, antenna temperature (corrected by opacity), source correction, antenna temperature flux ratio and aperture efficiency for Venus and Saturn at 86.2 GHz. All data were taken at 30 degrees elevation approximately. The last three columns are repeated: first one is not corrected by the membrane, second is corrected. Observations at 110 GHz were of very poor quality and should be taken with care.*

one was done with the polarizer and epoch two without the polarizer. The efficiency at 110 GHz, only available in the first epoch, is $\sim 12.5\% \pm 0.05$.

It is rather interesting to observe that the difference between forward efficiency and main beam efficiency is a factor of 3.5 at 87 GHz. Forward efficiency has improved after holography but the main beam efficiency has not increased as expected, and that is a direct consequence of the low efficiency aperture.

7 The surface error budget of the primary reflector

We can estimate the efficiency of the primary reflector from 14, and the surface errors of the primary reflector from equation 13. Table 7 summarizes both values for the 3 frequency intervals. We have used the average from Mars and Venus measurements to estimate the previous values for each interval of frequency.

λ μm	η_a	η_{m1}	σ μm
3500	0.21	0.37	280
3331	0.145	0.25	310
2997	0.125	0.22	293
2725	0.125	0.22	267

Table 7: *Wavelength, aperture efficiency, efficiency of the primary reflector and estimated RMS for the primary reflector surface from the Ruze's formula.*

Ideally, values for different frequencies and the same case (membrane corrected or not) should give the same σ for the error surface. However this does not happen as can also be seen

in Fig. 6, where we display the aperture efficiency as a function of frequency with and without the polarizer. The decrease with increasing frequency is steeper than expected from Ruze's formula, except for the 100 GHz data.

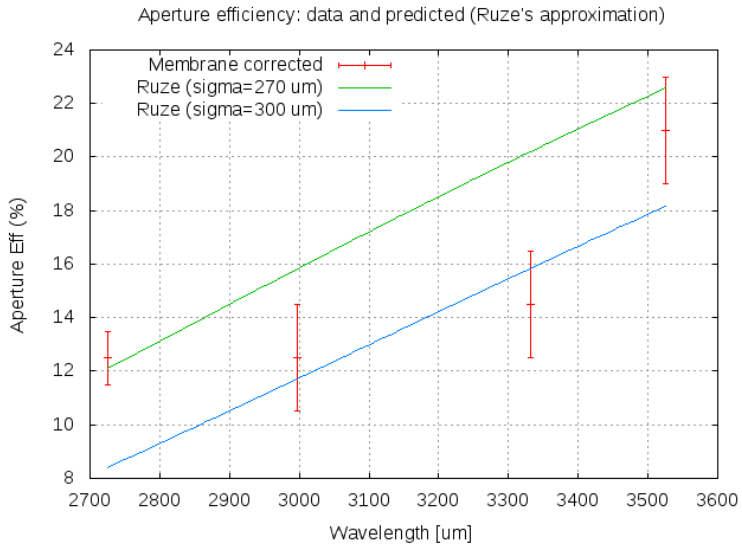

Figure 6: *Aperture efficiency versus wavelength*

Absolute values differ largely from the estimated 190 μm obtained by holographic measurements (see Lopez 2012).

8 Gain, position errors and HPBW versus elevation

We have obtained gain curves for the 40 m radiotelescope at 86, 90, 100 and 110 GHz. Fig. 7 shows the normalized gain as function of elevation from double pointing scans towards Venus, Mars, Saturn and 3C84 at 86 GHz. All scans were performed with automatic Z focus corrections from focus scans.

Fig. 7 shows some odd behaviours:

- The gain curve has a different behaviour for 3C84 and the planets. The gain curve peaks at 45 degrees elevation for the former, while it peaks at 30 degrees for the latter.
- The gain curve has a different trajectory when tracking planets upwards and downwards. Fig. 8 displays this effect more clearly. We have connected the values with lines so that it is easier to spot.
- The gain drops at the culmination on Mars and Saturn.

In Fig. 8 we show the normalized gain versus elevation for Mars at 90 and 100 GHz. We have connected the values with lines to show the trajectory upwards and downwards. The line

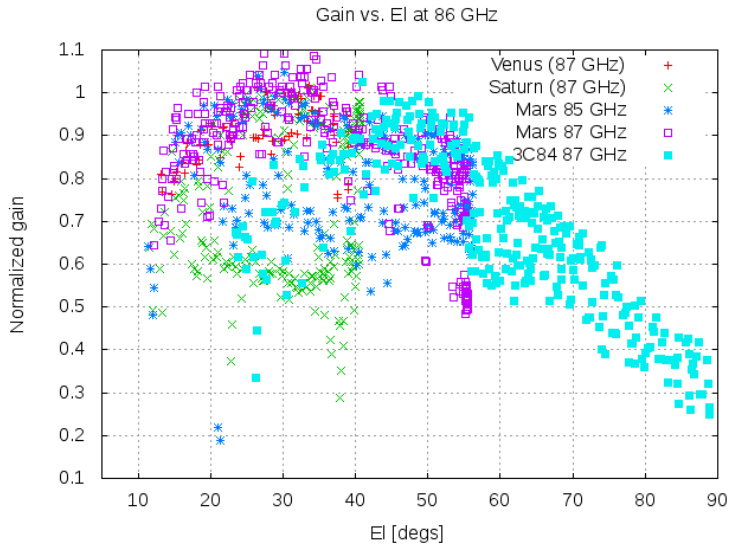

Figure 7: *Gain curve at 86 GHz.*

also displays a sawtooth behaviour which comes from the different intensity (∼5%) among the elevation and azimuth drifts. In order to check if this behaviour arises from an erronous computation of planet ephemeris we observed the upwards and downwards trajectory of the planets while making maps on the source. We intended to see if there were systematic pointing errors and if plotting the maxima of each map at different elevations the curve displayed the same upwards-downwards difference. All these observations were done with the polarizer removed.

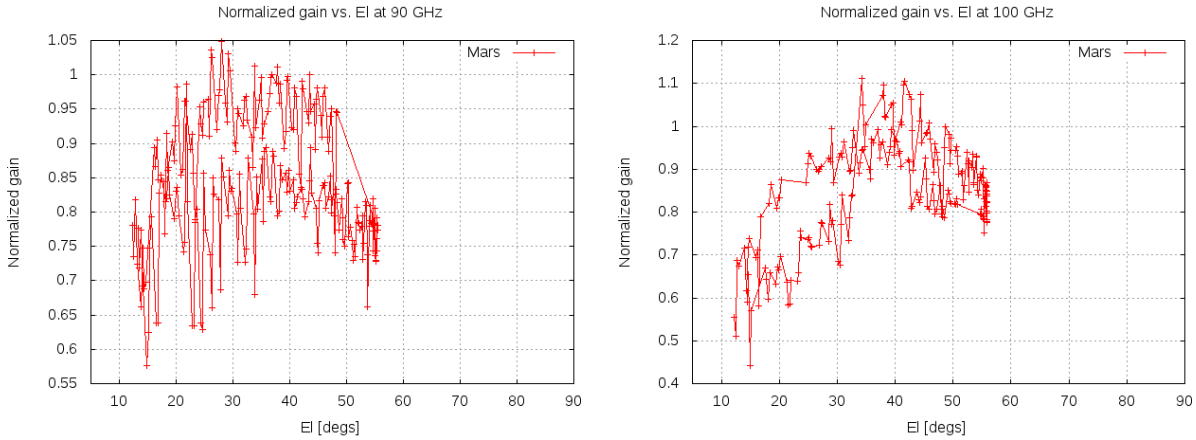

Figure 8: *Normalized gain versus elevation for Mars at 90 and 110 GHz. The values are connected by lines to show the different trajectory upwards and downwards. The saw tooth corresponds to the difference between azimuth and elevation drifts.*

Fig. 9 summarizes the results from such observations at 85, 90 and 100 GHz. Before each map, two pointing scans and one Z focus scan were performed. This figure displays the results from the pointing scans as a function of elevation. Figs. 10 show the position error of the fits.

We do not reproduce the systematic effect of the upwards - downwards gain difference seen previously. We have no explanation for the difference of behaviour seen in the observations done in the first epoch with the polarizer. We find odd that the polarizer be the cause since radiation from the planets is not polarized.

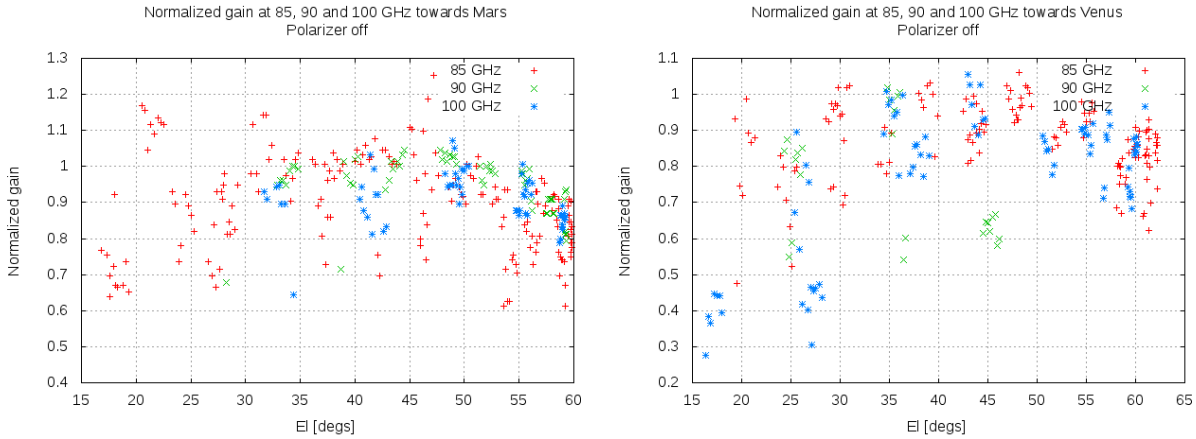

Figure 9: *Normalized gain versus elevation for Mars and Venus at 85, 90 and 100 GHz. Polarizer not installed*

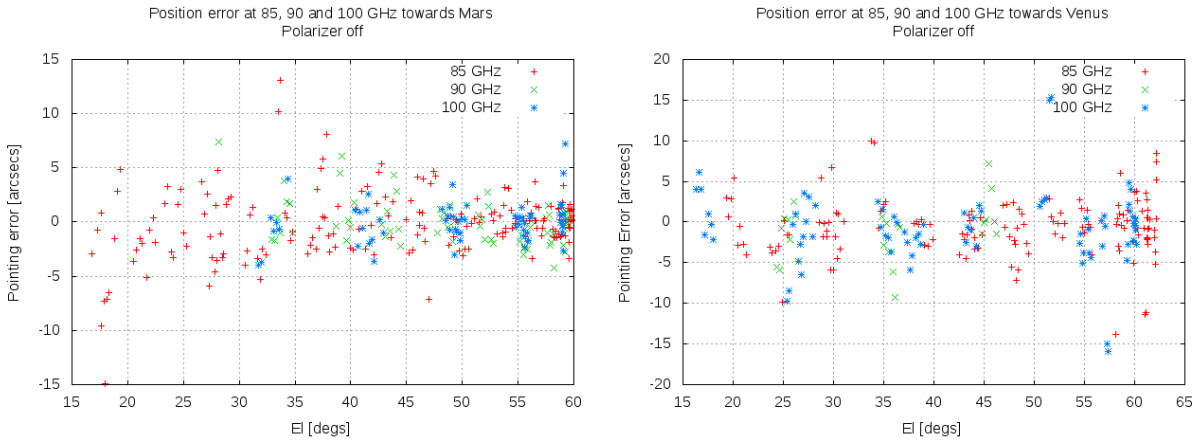

Figure 10: *Azimuth and elevation errors versus elevation for Mars and Venus at 85, 90 and 100 GHz. Polarizer not installed*

Pointing errors mostly stay below $\pm$ 3 arcsecs and do not show any systematic effect.

We have also investigated the dependence of the HPBW versus elevation. Fig. 11 displays the HPBW obtained from pointing fits towards Mars and Venus at different frequencies as a function of elevation. Mars shows a systematic effect: there is an increasing slope which depends on elevation. At 85 GHz the HPBW increases from 22 at 15 degrees elevation to 27 arcsecs at 60 degrees elevation, at 90 GHz the increase goes from 23.5 to 25 arcsecs and at 100 GHz from 21.8 to 22.8 arcsecs. Therefore the increase ranges from 4% to 20%. Surprisingly the increase rate is larger at lower frequencies. Venus does not show such a clear dependence on elevation.

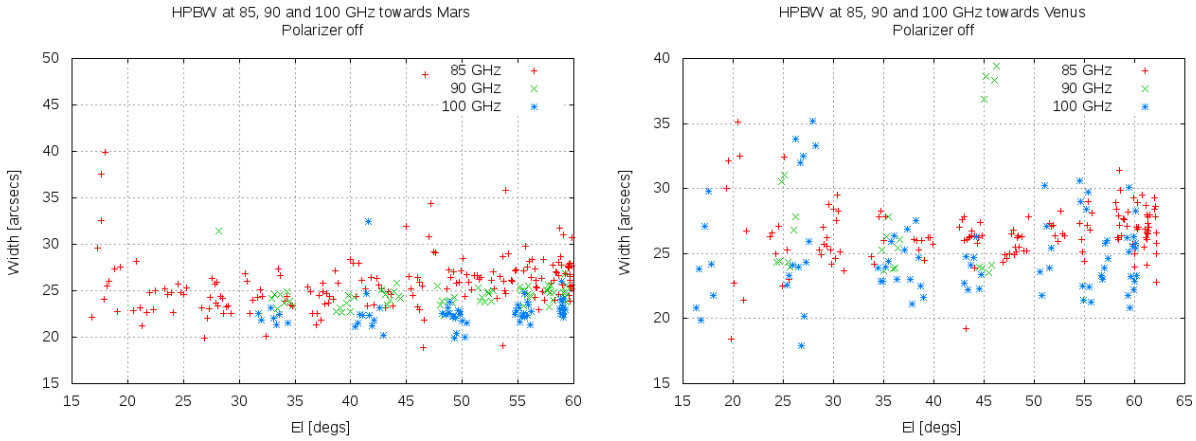

Figure 11: *HPBW versus elevation for Mars and Venus at 85, 90 and 100 GHz.*

We collect in table 8 the observed sources sizes for Mars and Venus along azimuth and elevation and the expected widths obtained convolving the source size with the beam of the telescope. We have assumed a taper of 0.2 to estimate the HPBW of the telescope. To compute the convolution of a disc source with a gaussian we have used the following approximation (Baars, 2007):

$$\theta_{exp} = \sqrt{\theta_b^2 + \frac{\ln 2}{2}\,\theta_s^2}$$

where θ_{exp} is the expected size, θ_b the Half Power Beamwidth of the telescope and θ_s the source size.

θ_b	θ_s	θ_{exp}	θ_{obs}	θ_s	θ_{exp}	θ_{obs}
	Mars			Venus		
21.3”	13.8”	∼22.8”	24.5± 2	18.3”	∼23.9”	27.5”
20.5”	13.8”	∼22.0”	24.2±0.8	18.3”	∼23.1”	26”?
18.5”	13.8”	∼20.2”	22.3±0.5	18.3”	∼21.4”	25”

Table 8: *HPBW of the telescope, source sizes, expected size from convolution, and observed width determined from azimuth and elevation drifts towards the source*

We conclude that, if the taper assumption is correct, the expected widths are $\sim 10\%$ smaller than the observed ones for Mars and 16% smaller for Venus. According to Baars an axial defocusing increases very slightly the width and therefore is not a reliable tool to determine defocus along Z. In any case we have studied the behaviour of the focus at 3 mm in the next sections.

9 Focus along Z

All observations, double pointing scans and maps, have been performed after running a focus scan along the Z axis to obtain the optimum Z focus which maximizes detected power. The focus scan consists on moving the subreflector along the Z axis $\sim$ 11 mm between -7 mm and 4 mm approximately while tracking the source. A typical result is shown in Fig. 12, where Ta* is depicted versus relative focus along Z at an observing frequency of 100 GHz. Ta* is maximum at -1.4 mm and it drops to half power at a focus distance of 3.6 mm approximately. The wavelength at 100 GHz is 3 mm and hence we conclude that a shift of 1 wavelength along Z causes the intensity to drop dramatically (to half the maximum).

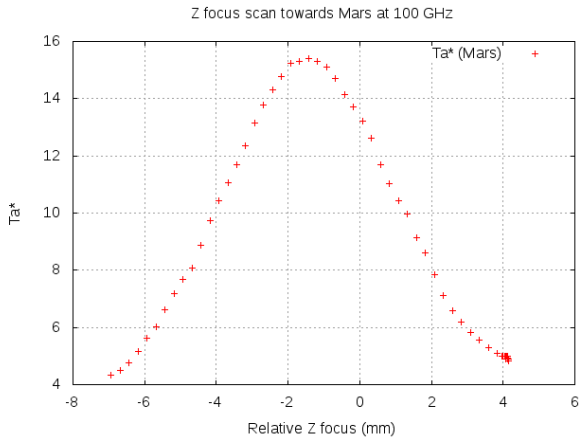

Figure 12: *Antenna temperature versus relative focus along Z at 110 GHz towards Mars.*

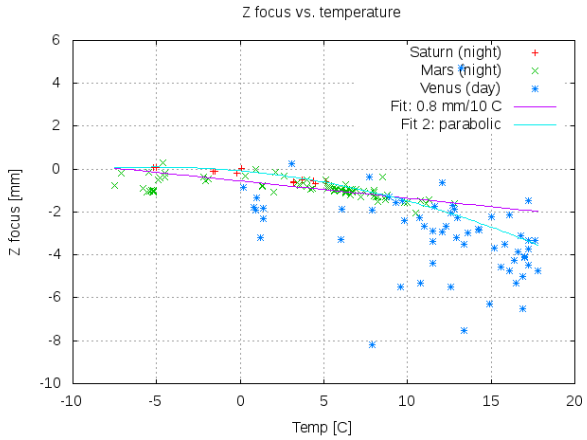

Figure 13: *Relative focus along Z versus temperature. Venus was observed during the day while Mars and Saturn were observed during night time.*

Hence observations at 3 mm requiere continuous checking of the focus towards strong

sources. Unfortunately the 40 m does not have neither beam switching nor wobbler switching and observations have to be performed in total power with good weather and strong sources.

We have investigated the influence of temperature in the focus in all scans performed at 85, 90, 100 and 110 GHz. Results are summarized in Fig. 13. This figure displays the best Z fit for each scan as a function of temperature. Data from Mars and Saturn were obtained during the night while data from Venus was obtained during the day. We think that the dependence with temperature is better seen for Mars and Saturn since the structure of the subreflector and the tetrapod legs are in an environment with small temperature gradients. During the day the sun rays impact directly onto the structure and cause the legs to stretch in a non uniform way, also shifting the focus in Y and X. This is the most probable cause of the spread of data from Venus.

10 Focus along Y and X. New observations

In order to look for the best focus position along the X and Y axis, we made double pointing scans at 7 different positions of the subreflector along these axis. The advantage of this method over doing focus scans is that pointing corrections are automatically taken into account. Focus scans while tracking a source are useless since the pointing and the intensity of the line change with focus. Observations were done at 85 GHz at night towards Mars to avoid the effects of direct sun exposition on the subreflector and tetrapod legs.

We have estimated the best focus fit by finding the pointing drift which minimizes the intensity of the secondary lobes and maximizes the intensity of the main beam. Fig. 14 shows one of the most clear examples of the series. The secondary lobe gets larger for some values of the focus along the Y axis.

Results from observations were noisy and at some elevations it is difficult to determine which Y position is best. However there is a trend which is visible in Fig. 15 where we plot the optimum Y focus as a function of elevation. Below 40 degrees the best Y focus position is 6 mm. Between 40 degrees and 60 degrees (the elevation at which Mars culminates), the optimum Y fit shifts to -6 mm.

In order to check if a correction of +6 mm of the subreflector along the Y axis at all elevations is adequate we did some pointing scans and maps towards Mars on march 20th at 85 GHz. Maps are shown in next section.

The correction works very well below 40 degrees elevation since the secondary lobe upwards disappears completely. However there is a secondary lobe almost all around the main beam at 60 degrees elevation. The lobes are asymetric and display a maximum towards negative Y and X offsets. This maximum apparently shifts slightly towards the X axis with elevation. A similar maximum but less important was seen without the Y correction. See next section on maps for the maps.

An unexpected consequence arises from the subreflector fit along Y axis: the gain curve no longer has a maximum at 35 degrees elevation. Now it haves a very similar aspect to the 22 GHz one which still requires further study (de Vicente 2010b). According to Fig. 16 the gain curve is a straight line which peaks at 15 degrees elevation. This increase of gain at low elevations does not affect the aperture efficiency computed in section 6 in the interval of 30 to 40 degrees elevation.

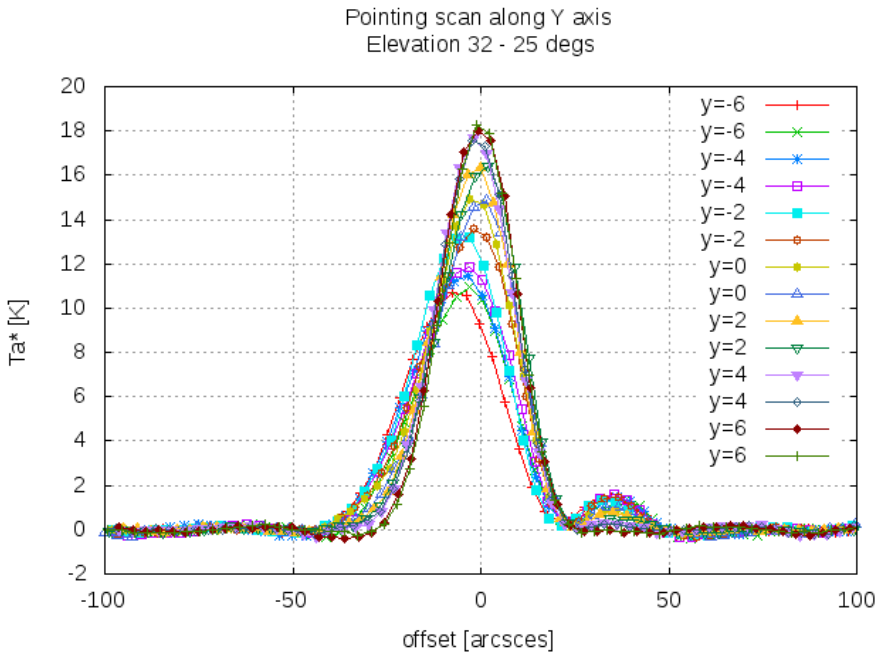

Figure 14: *Pointing scan along elevation at different positions of the focus along the Y axis.*

Figure 15: *Best Y focus offset obtained from double ponting scans and minimizing the secondary lobe and maximizing the main beam intensity.*

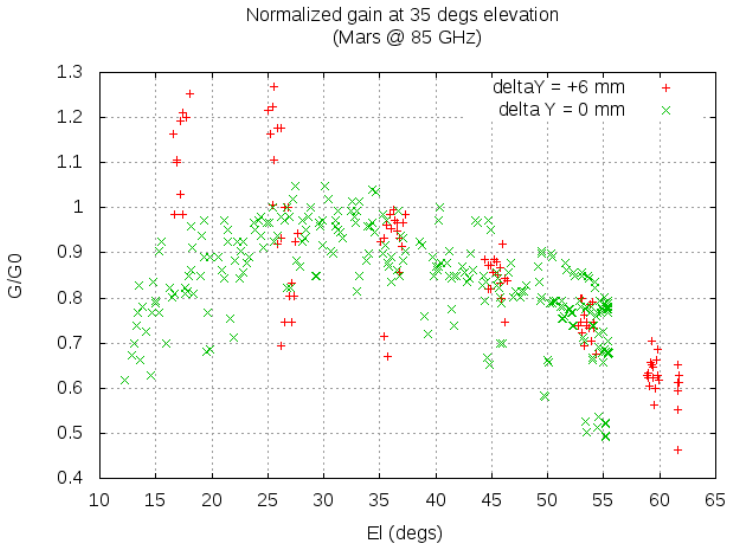

Figure 16: *Pointing scan along elevation at different positions of the focus along the Y axis.*

If we accept that efficiency is maximum at 15 degrees elevation the aperture efficiency of the antenna should be multiplied by 1.2 and we get a value of $\sim$0.25.

Results for X axis were noisier and less concluyent. These observations hsould be repeated in the future.

11 Source maps

We have performed continuum maps towards Mars and Venus at 86, 90 and 100 GHz at different elevations and with two different setups: a constant focus offset of +6 mm along the Y axis and the current focus dependence. All observations were done at night.

Fig. 17 shows the aspect of the beam towards Mars and Saturn at low elevations with the current Y focus curve. Figs. 18 to 20 show the maps towards Mars with the current Y focus fit on the left panels and with an offset of +6mm on the right panels.

Finally 21 shows maps towards Mars at 90 and 100 GHz at the an elevation of 56 degrees.

Maps at low elevation show a secondary lobe above the main beam that probably comes from a wrong focus along the Y axis. The lobe disappears at elevations above 40 degrees. However at elevations between 50 and 60 degrees a weaker lobe appears below the main beam. When we use an offset of +6 mm the secondary below the main beam is stronger. It seems that at high elevations the focus should be shifted towards negative values. This behaviour is consistent with the focus fit offset along Y axis in previous section. We believe that the Y focus position dependency on elevation is not optimal and requires a correction like the one in Fig. 15.

Fig. 20 also shows that the secondary lobe is slightly shifted towards negative azimuths and this possibly requires a small negative shift of the focus along the X axis.

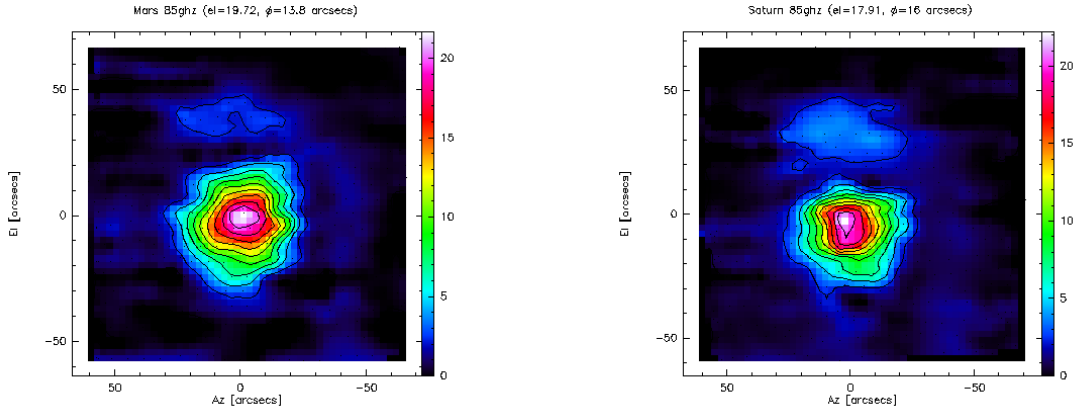

Figure 17: *Mars at 19 degrees elevation and Saturn at 17 degrees elevation.*

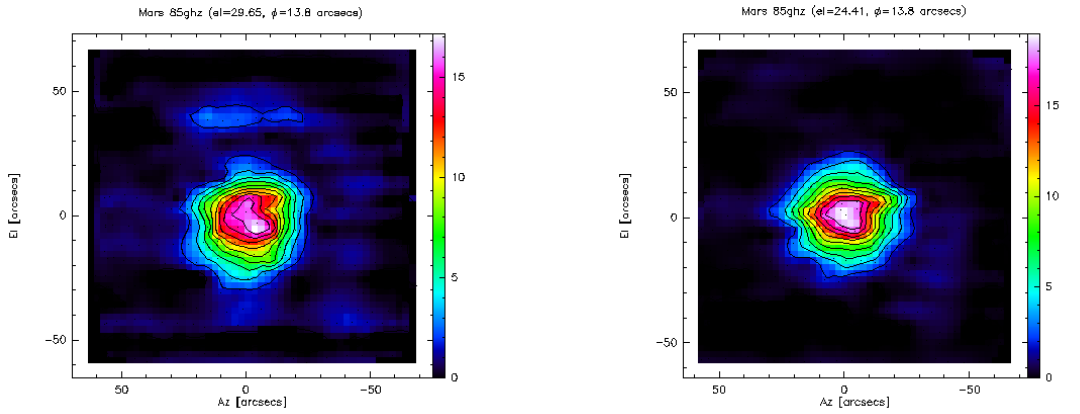

Figure 18: *Continuum maps towards Mars at approximately 26 degrees elevation with focus positions: y=0 (left) and y=+6mm (right).*

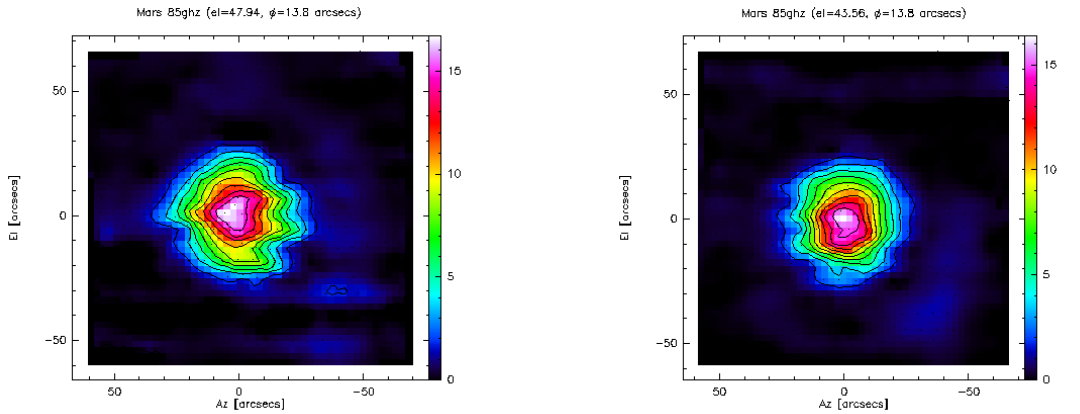

Figure 19: *Continuum maps towards Mars at approximately 43 degrees elevation with focus positions: y=0 (left) and y=+6mm (right).*

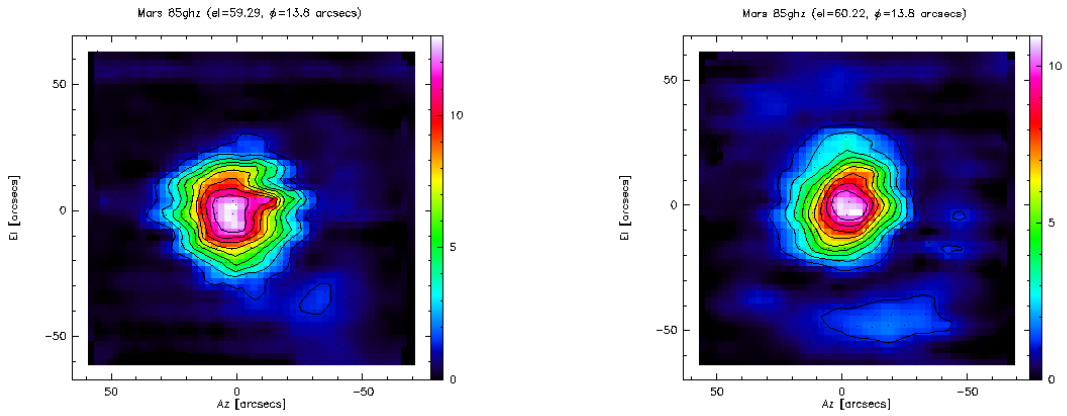

Figure 20: *Continuum maps towards Mars at approximately 60 degrees elevation with focus positions: y=0 (left) and y=+6mm (right).*

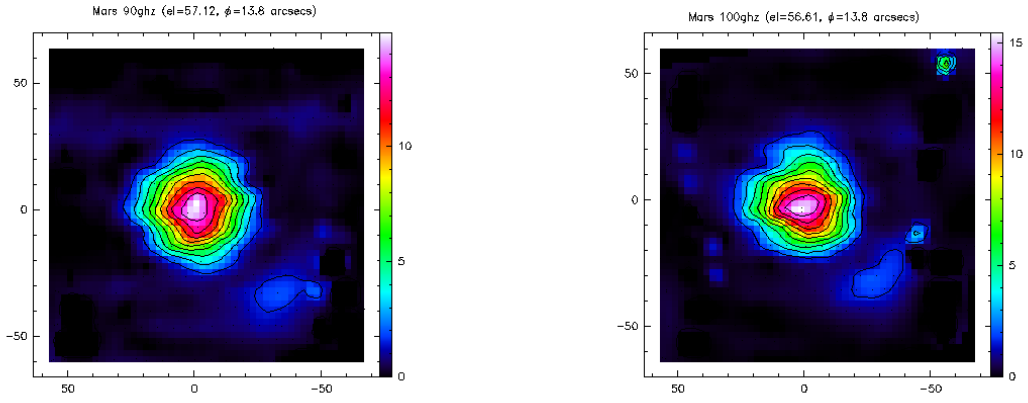

Figure 21: *Continuum maps towards Mars at approximately 56 degrees elevation with focus positions: y=0 at 90 (left) and 100 GHz (right)*

12 Conclusions

- The aperture efficiency of the antenna has improved since 2010 after several surface adjustements:

Date	η_a	Notes
27-04-2010	0.093 ± 0.01	Original surface
18-04-2011	0.125 ± 0.01	New membrane
02-10-2011	0.15 ± 0.01	First surface adjustment
01-03-2012	0.21 ± 0.01	Second surface adjustment (1)

Table 9: *Evolution of the aperture efficiency at 85 GHz at the 40 m dish with time. (1) If we consider that the maximum efficiency is achieved at 15 degrees elevation with a better Y focus, the aperture efficiency is 0.25*

- We have estimated the forward efficiency, aperture efficiency and main beam efficiency of the 40 m radiotelescope in the 85 to 110 GHz range. We also estimate the efficiency of the polarizer and of the vertex membrane. We summarize these values in table 10.

η_f	η_a	η_{mb}	η_m	η_p
0.85	0.21	0.25	0.94	0.96

Table 10: *Parameters at 85 GHz: forward efficiency, aperture efficiency, main beam efficiency, vertex membrane efficiency and polarizer efficiency.*

- The estimate for the RMS of the primary reflector is ~ 270 μm and differs very much from the holography estimate of 190 μm.
- With the current focus adjustment the gain peaks at elevations between 35 and 50 degrees. The gain curve seems to differ between planets and 3C84.
- Beam widths are 10% to 16% larger than the expected ones from convolving the beam of the telescope with angular source width.
- Beam widths depend linearly on elevation. The width increases between 4% and 20% from 15 degrees elevation to 60 degrees elevation.
- The focus along the axial axis varies with the environment temperature and the direct exposition of the sun on the subreflector and tetrapod legs.
- The focus along the Y axis is not optimum and requires some corrections at elevations below 40 degrees and above 50 degrees.
- The focus along the X axis also requires some correction at elevations above 50 degrees.

- The gain curve peaks at 15 degrees elevation if a new focus along the Y axis is applied. The aperture efficiency in that case increases to 0.25 and the estimated RMS for the primary reflector drops to 215 μm, which is only 13% higher than obtained from holographic measurements.

Further studies on the focus of the antenna at 3 mm are required. A new pointing model and gain curves should be obtained once the focus corrections are applied. We also plan to study the behaviour of the beam witdh as a function of elevation and gain curves for planets and non-planet sources.

References

[Cordobes 2009] D.Cordobés, J.A.López Pérez, C.Almendros, J.A.Abad, J.M.Yagüe, S.Henche. "Diseño, montaje y medida de la unidad de FI del receptor de 3mm". IT OAN 2009-4

[Lopez 2012] J.A. López Pérez, Private communication. 2012

[Malo 2010] I. Malo, J. D. Gallego, M. Diez, I. López, R. García. "Medida de la Permitividad a temperaturas criogénica y ambiente con el método de Perturbación de Cavidad". IT OAN 2010-9

[de Vicente 2010b] P. de Vicente. "Pointing models for the 40 m radiotelescope at 6, 8 and 22 GHz". IT-OAN 2010-11

[de Vicente 2010a] P. de Vicente, R. Bolaño, J. A. López Fernández, J. A. López Pérez, F. Tercero. "Preliminary results of the 40 m radiotelescope at 88 GHz". IT-OAN 2010-16

[de Vicente 2011] P. de Vicente, F. Tercero, T. Finn, J.A. Abad, J. Fernández, J.M. Yagüe. "Installation and measurements of efficiency for the new membrane at the vertex of the 40m radiotelescope". IT-OAN 2011-4